ELSEVIER ELSEVIER

Contents lists available at ScienceDirect

Acta Materialia

journal homepage: www.elsevier.com/locate/actamat



Magnetic domain-twin boundary interactions in Ni-Mn-Ga

Medha Veligatla^a, Carlos J. Garcia-Cervera^{b,c}, Peter Müllner^{a,*}

- ^a Boise State University, Boise 83725, USA
- ^b University of California, Santa Barbara 93106, USA
- ^c Visiting Professor at BCAM Basque Center for Applied Mathematics, Mazarredo 14, E48009 Bilabo, Spain



ARTICLE INFO

Article History: Received 11 September 2019 Revised 24 March 2020 Accepted 25 March 2020 Available online 30 April 2020

Keywords: Magnetoelastic defect Micromagnetics Twin microstructure Twin thickness Strength

ABSTRACT

The stress required for the propagation of twin boundaries in a sample with fine twins increases monotonically with ongoing deformation. In contrast, for samples with a single twin boundary, the stress exhibits a plateau over the entire twinning deformation range. We evaluate the twin boundary and magnetic domain boundary interactions for increasing twin densities. As the twinned regions get finer, these interaction regions result in additional magnetic domains that form magnetoelastic defects with high magnetostress concentrations. These magnetoelastic defects act as obstacles for twinning disconnections and, thus, harden the material. Whereas in a low twin density microstructure, these high-energy concentrations are absent or dilute and their effectiveness is reduced by the synergistic action of many twinning disconnections. Therefore, with increasing twin density, the interaction of twin boundaries and magnetic domain boundaries reduces the twin boundary mobility. The defect strength has a distribution such that twinning disconnections overcome soft obstacles first and harder obstacles with ongoing deformation. The width of the distribution of obstacle strength and the density of obstacles increase with increasing twin density and, thus, the hardening coefficient increases with increasing twin density.

© 2020 Acta Materialia Inc. Published by Elsevier Ltd. All rights reserved.

1. Introduction

Shape memory alloys are materials, which undergo diffusionless transformation (martensitic transformations) and exhibit strain reversal with the application of mechanical or thermal energy. The thermal energy promotes deformation while the material is heated through martensite-austenite transformation. Ni-Mn-Ga belongs to a class of magnetic shape memory (MSM) alloys that undergo deformation by means of heat, mechanical stress, and magnetic field. While the deformation through heating/cooling occurs through crystallographic reorientation between austenite and martensite phases, the mechanical stress or a magnetic field promotes the deformation by crystallographic reorientation within the martensite state. Ni-Mn-Ga has multiple martensite variants and it is magnetically anisotropic, with the c-axis as the easy axis of magnetization [1,2]. When a mechanical stress/magnetic field induced deformation takes place, the magnetic orientation depends on the orientation of the c-axis in the martensite variant [3]. The mechanism of this deformation in Ni-Mn-Ga MSM alloys is twinning [4]. While twinning occurs, the regions on either side of the twin boundary have different crystallographic orientations. Thus, twin domains have different magnetization orientations across the twin boundary. While the material is deforming, the twin boundary propagates across the sample and crystallographic reorientation takes place. One twin region grows at the expense of the other. This crystallographic reorientation can take place with a single twin boundary or with many twin boundaries moving simultaneously. The amount of deformation in the MSM alloy is typically quantified by conducting uniaxial compression test. Many research groups have characterized the mechanical properties of these MSM alloys with and without a magnetic field [5–8]. Other research groups have studied the magnetic domains [9–15] and twin boundary structure, type, and mobility [15–20].

Before the research in magnetic shape memory alloys steered towards the study of twin boundaries in Ni–Mn–Ga, Straka et al. [21,22] studied the mechanical behavior of these alloys by varying the number of twin boundaries in the sample. The experimental results showed that the sample with many twin boundaries required higher stress compared to the sample with a single twin boundary to move the twin boundaries through the sample. In addition, the stress monotonically increased with increasing strain for the sample with many twin boundaries, i.e. the samples exhibit work hardening (Fig. 1, [21]). In contrast, there is a stress plateau for the sample with a single twin boundary. Later as the research advanced in the MSM field, it was recognized that the twin boundaries in Ni–Mn–Ga can be classified into Type I and Type II. In 2016, Heczko et al. [23] studied the mechanical behavior of Ni–Mn–Ga alloys with single type I, single type II, and fine twins. Again, the stress-strain curves for single twin

^{*} Corresponding authors.

E-mail address: petermullner@boisestate.edu (P. Müllner).

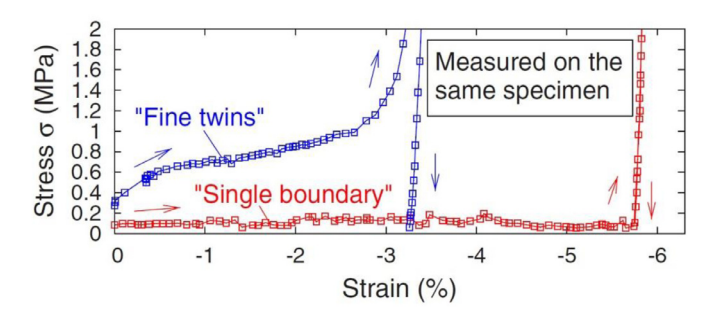


Fig. 1. Stress—strain curves for a sample with a single twin boundary (red) and with fine twins (blue). The sample with only one twin boundary exhibits a stress plateau at about 0.1 MPa. The sample with fine twins exhibits work hardening over a stress range from 0.4 to 2 MPa. Reproduced from [20] with permission of the American Institute of Physics. (For interpretation of the references to color in this figure legend, the reader is referred to the web version of this article.)

boundary exhibited plateau while for the fine twin boundaries the stress increased monotonically. Researchers speculated that the interaction of twin boundaries with magnetic defects or mutual interactions of differently oriented twins caused this work hardening [23]. The work hardening affects functional properties of magnetic shape memory alloys such as the magnetic switching field and hysteresis losses. Understanding these properties will aid the design of MSM actuators and sensors.

In the present study, we evaluate these twin boundary and magnetic domain interactions for increasing twin density in Ni–Mn–Ga sample by using micromagnetic simulations. We use a code developed by Garcia-Cervera [24]. Hobza et al. used this code to study magnetic torque phenomena in Ni–Mn–Ga [25]. Here, we add magnetic energy mapping to this code to identify the structure and energy of defects resulting due to the interaction of magnetic domains and twin boundaries. The results show that the interaction of magnetic domain boundaries and twin boundaries cause the hardening of fine twinned Ni–Mn–Ga.

2. Micromagnetics

In the present study, we simulate the domain evolution using micromagnetics. We obtain the equilibrium magnetic state with respect to time with a fixed twin microstructure, i.e. with static twin boundaries. Studying the static twin boundary state allows us to investigate greater details at interaction sites of magnetic domains and twin boundaries. Garcia-Cervera [24] developed this micromagnetics code and Hobza et al. [25] applied it to Ni-Mn-Ga system to study the torque generated by a magnetic field on samples with various twin microstructures. This code evaluates the Landau-Lifshitz equation. In our method, we solve linear systems of equations with constant coefficients. The cost per step of our method is O(N log N), where N is the number of cells. Using this customized micromagnetics code we obtained magnetic energies for magnetic equilibrium structures at varying twin densities in Ni-Mn-Ga. The equilibrium magnetic structures and energies obtained through these simulations take into account the anisotropy, exchange, stray field, and Zeeman energies. The code solves the following Landau-Lifshitz-Gilbert equation to approach the minimum energy state:

$$d\mathbf{M}(\mathbf{r})/dt = -\mu_0 \gamma \mathbf{M} \times \mathbf{H} - \alpha(\mu_0 \gamma / M_s) \mathbf{M} \times [\mathbf{M} \times \mathbf{H}]$$
 (1)

where $\mathbf{M}(\mathbf{r})$ is the magnetization density at position \mathbf{r} , γ is the gyromagnetic ratio, α is the dimensionless damping parameter, and $\mathbf{H}(\mathbf{r})$ is the magnetic field, which is the negative derivative of total energy with respect to magnetization:

$$\mathbf{H} = -\frac{\delta E}{\mu_0 \delta \mathbf{M}} = -\left(2K_u/\mu_0 M_s^2\right)(M_2 + M_3) + \left(2C_{ex}/\mu_0 M_s^2\right)\Delta \mathbf{M} - \nabla \mathbf{U} + \mathbf{H}_{ext}$$

where K_u is the anisotropy constant, M_s is the saturation magnetization, M_2 and M_3 are magnetization components that are orthogonal to the axis of easy magnetization, C_{ex} is the exchange constant, μ_0 is magnetic permeability of free space and \mathbf{H}_{ext} is the external magnetic field.¹ The individual summation terms in Eq. (2) are the energies associated with magnetocrystalline anisotropy, exchange interaction, stray field and external magnetic field. In the present study, we evaluate the evolution of magnetic domain structures to study the twin boundary motion in the absence of an external magnetic field. Therefore, the Zeeman energy term is neglected in this calculation (i.e. $\mathbf{H}_{\text{ext}} = 0$). While the other energy terms are briefed as follows: magnetocrystalline energy is the energy associated with the orientation of magnetic domains with respect to the axis of easy magnetization, the exchange energy is the short range interaction energy between neighboring magnetic moments, and the stray field is associated with magnetic domain splitting. A detailed description of these energy terms and the micromagnetics code is given in [25].

3. Numerical simulation

We studied the effect of twin boundary density on hardening by increasing the twin density and evaluating the distribution of magnetic moments and their resulting magnetic energies. We conducted micromagnetic simulations to obtain the magnetic energies and equilibrium magnetic structures to evaluate the magnetic domain and twin boundary interactions. The twin densities were varied from a minimum of 1.7 μ m⁻¹ to a maximum of 47 μ m⁻¹ on samples with 1 to 5% strain (with 1% increments) i.e. elongating the sample. The sample sizes used to conduct this study varied from 1.56 μ m imes 0.53 μ m \times 0.36 μ m (1% strain) to 1.63 μ m \times 0.50 μ m \times 0.36 μ m (5% strain). Therefore as the sample dimension changes with strain the minimum and maximum twin density at each strain percent is slightly different. The number of twin boundaries in a sample where systematically increased from lowest twin density with one twin boundary to the highest twin density with 65 twin boundaries. While doing so, the fractions of regions with the c-axis (axis of easy magnetization) parallel and perpendicular to the sample length were determined from the strain on the sample. Throughout the sample length, the twin boundaries were inclined at 45° with the sample edge and the direction of easy magnetization (which corresponds to the crystallographic c axis) across these twin boundaries were defined to be 90°. The schematic representation of the simulation set up for a single twin boundary system and a dense twin boundary system is shown in Fig. 2. The horizontal and vertical lines within the twinned regions represent the preferred direction of magnetization, which are nearly 90° across the twin boundaries. The volume of the simulation sample was divided into 384 cells along the longest dimension and 192 cells along the intermediate dimension, making it 73728 cells in total. Therefore, the dimension of each cell is \sim 4.06 nm \times 2.7 nm (at 1% strain) and each of these cells has an assigned magnetization vector. In these simulations, we used a saturation magnetization M_s of $4.85 \times 10^5 \text{ A/m } (\mu_0 M_s = 0.61 \text{ T})$ [26]. This defines the magnetic moment per cell as done in previous studies [25]. Each simulation ran for 20,000 iterations. Therefore, to obtain a magnetic structure with minimum energy configuration, we added multiple runs that continue from the previously ended run, making it 180,000 iterations. The individual magnetic energy contributions (anisotropy, exchange, and stray field energy) for the equilibrium state were also obtained during these simulations. All the magnetic energies and domain structures for the equilibrium states obtained for this study were generated in the absence of an external magnetic field.

¹ Equations 1 and 2 are given in SI unites and differ from those given in Ref. [24].



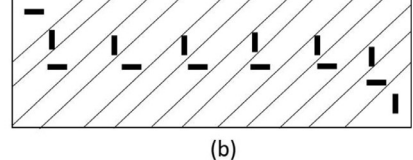


Fig. 2. Schematic of the sample with (a) single twin boundary and (b) dense twin boundary microstructure. The horizontal and vertical lines represent the orientation of the *c*-axis (axis of easy magnetization) and the twin boundaries are inclined at 45° to the edge of the sample.

4. Results

Fig. 3 shows the magnetic energy density maps for twin densities ranging from 1.7 to 47 μ m⁻¹ for samples with 1–5% strain. For low twin densities (up to about 5 μ m⁻¹), the calculated energies did not differ significantly. Therefore, the energy values appeared scattered with no particular trend. At higher twin densities (from about 8.4 to 47 μ m⁻¹), for samples with 2, 3, and 4% strain, the energy density increased linearly with increasing twin density and with increasing strain. In contrast, for samples with 1 and 5% strain, the energy density regressed at higher twin density. This non-linear dependence was due to the magnetic resolution dependence on the cell size. With a 384 \times 192 cell size, at 1 and 5% the finest twinned regions (i.e. the region between two twin boundaries) were about 12.5 nm wide, which is equivalent to a magnetic domain wall size [27]. At this scale, there were only 3 cells in the twinned region (cell size at 1% strain = 4.06 nm x 2.7 nm) i.e. the actual rotation of magnetic moments within one cell was large such that the averaging of magnetic moments within one cell lead to large errors. The averaging of magnetic moments in one cell resulted in incorrect magnetic domain patterns when the twin width correlated with the magnetic domain wall thickness. This was the case for 1 and 5% strain at large twin density. However, due to different strains affecting the twin width in our simulations, the smallest twin width for the strains 2 and 4% is ~20 nm and for 3% is ~24 nm, which are larger than the domain wall size. For 1, 2, 4, and 5% strain, the twin domains with *c* parallel and perpendicular to the sample axis have different thickness. In these cases, the minimum twin width of 12.5 nm (1 and 5% strain) and 20 nm (2 and 4% strain), respectively, is smaller than the average twin width. For 3% strain all twins have the same thickness.

We performed 40 simulations including 8 twin densities for each strain state ranging from 1% to 5% with 1% increments. From these we selected the sample with 3% strain to demonstrate the magnetic structures. Fig. 4 shows the equilibrium magnetic domain structures for twin densities ranging from 1.7 (Fig. 4a) to 44.1 μ m⁻¹ (Fig. 4h) for a sample with 3% strain. Colors red (\leftarrow), blue (\rightarrow), yellow (\uparrow) and green

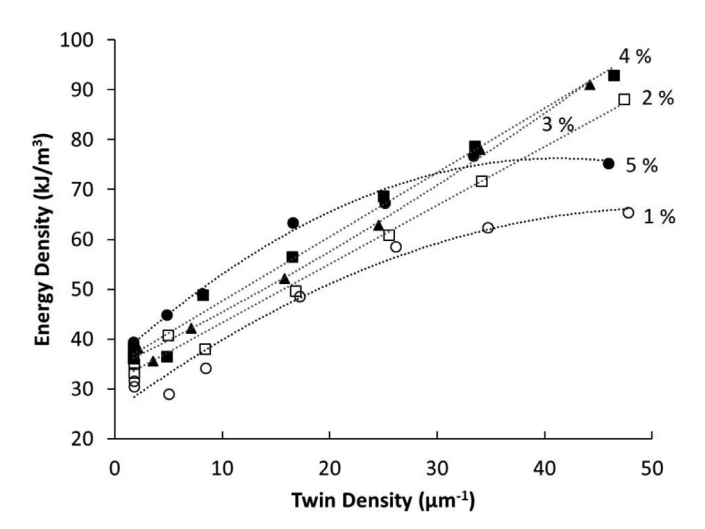


Fig. 3. Plot of total magnetic energy densities as a function of increasing twin density for samples with 1-5 % strain with varied twin densities from 1.7 to 47 μ m⁻¹.

(↓) represent the direction of magnetic moments. At lower twin densities, from Fig. 4a to d (i.e. $1.7-7.1 \mu m^{-1}$) the magnetic structures formed 90° domains across the twin boundary and 180° domains within the twinned regions resulting in a staircase like magnetic domain pattern across the twin boundaries. These results agree with the experimental characterization of magnetization with magnetooptics reported by Söderberg et al. [10]. At higher twin densities, as the twinned regions became thinner i.e. going from 15.7 to 24.5 μm^{-1} twin density (Fig. 4e and f) these staircase like transition regions moved towards the sample edges and became less prominent. The center of the sample had twinned regions with single magnetic domains separated by 90° domain walls across the twin boundaries. As the twinned regions got even finer (33.9 and 44.1 μ m⁻¹) additional vertical magnetic domains appeared that were perpendicular to the sample length (Fig. 4g and h). The formation of these vertical magnetic domains at higher twin densities for 2 and 4% strains are shown in Appendix A. Fig. 5 shows the contribution of each magnetic energy term (anisotropy, exchange, and stray field energy) towards the total magnetic energy for these equilibrium structures (at 3% strain). With increasing twin density (from 1.7 to 44.1 μ m⁻¹) the anisotropy and exchange energy increased monotonically while the stray field energy remained about constant, and the anisotropy energy contributed the most to the total magnetic energy. Fig. 6 shows the equilibrium magnetic domain structure for a single twin boundary system. The colors in the figure represent the orientation of magnetic moments indicated by the arrows. In the twin domain with c horizontal, a 180° magnetic domain boundary extended from the twin boundary to the surface of the sample. This magnetic domain boundary connected with another 180° magnetic domain boundary in the twin domain with *c* vertical. Additional vertical 180° magnetic domain boundaries extended from surface to surface. These results agree with the experimental Kerr microscopic images reported by Perevertov et al. [28] and Heczko et al. [29]. Closure domains formed where 180° magnetic domain boundaries reached the surface. A region on a magnetic domain boundary and the region at the intersection of magnetic domain and twin boundary are magnified in the top two figures. The arrows in these magnified regions show the orientation of magnetic moments. The regions on either side of the twin boundary formed 180° magnetic domains. These 180° domain walls contain multiple magnetic vortices. The magnetic energy distribution (i.e. the contribution from anisotropy, exchange and stray field energies to the equilibrium state) of a selected region at the intersections of the twin boundary and magnetic domain boundaries is represented in Fig. 7. The anisotropy and exchange energies were heightened at the twin boundary and at the domain boundary. At the twin boundary, the energies were about 100 kJ/m³, at magnetic domain boundary about 200 kJ/m³, and within the magnetic domains, the energies were less than 25 kJ/m³. Whereas the stray field energy was less than 25 kJ/m³ throughout the sample.

As the twinned regions became finer, additional magnetic domains formed that were perpendicular to the sample length. In such an equilibrium magnetic domain structure, there were regions where the twin boundaries interacted strongly with the vertical magnetic domain boundaries and there were regions where the twin boundaries did not or only weakly interact with the vertical magnetic domains. Fig. 8 is the equilibrium magnetic domain structure for such a dense twin boundary system. A region from a regular twin

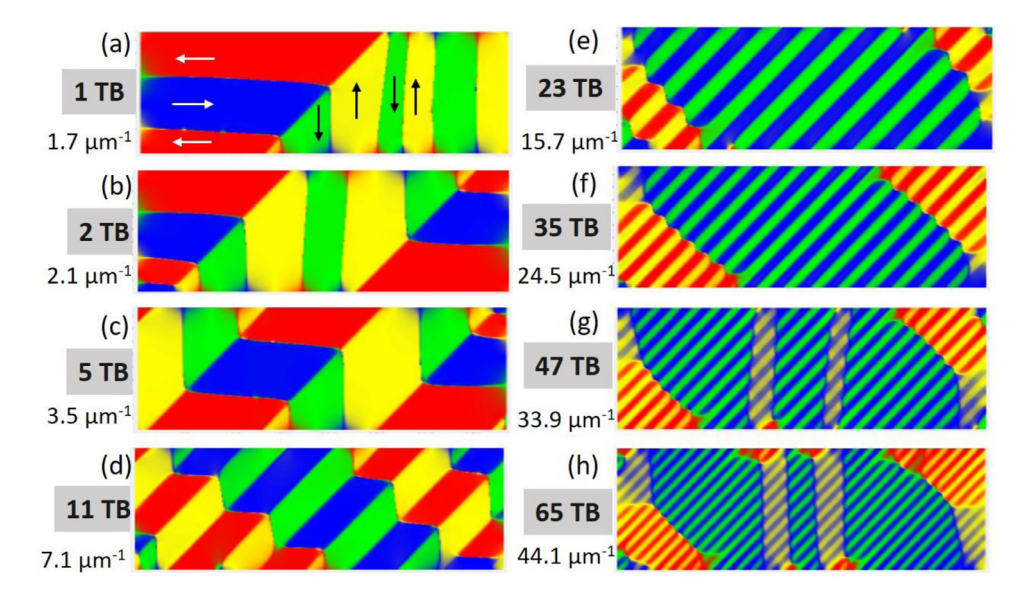


Fig. 4. The evolution of equilibrium magnetic domain structures of Ni-Mn-Ga at 3% strain with increasing twin density from 1.7 to 44.1 μ m $^{-1}$. The colors red (\leftarrow), blue (\rightarrow), yellow (\uparrow), and green (\downarrow) in the figures represent the direction of magnetic moments. (For interpretation of the references to color in this figure legend, the reader is referred to the web version of this article.)

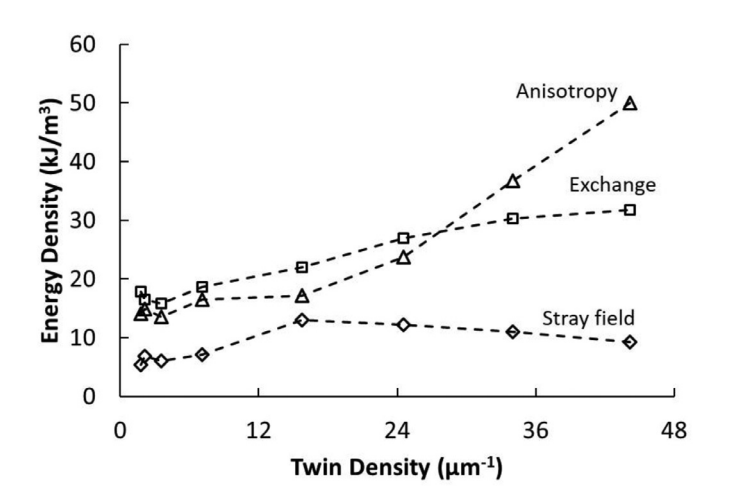
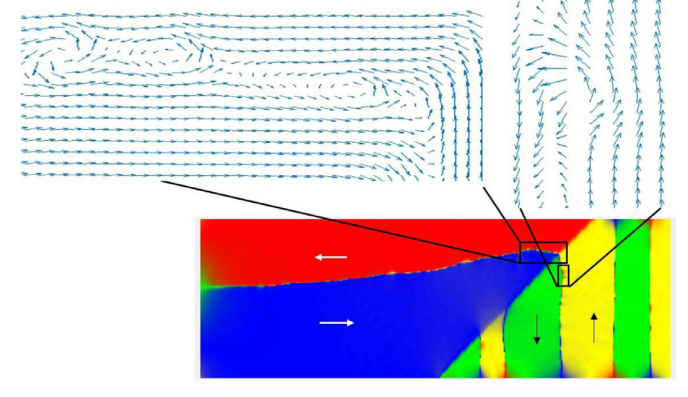


Fig. 5. Plot of anisotropy, exchange and stray field energy densities with increasing twin density for Ni-Mn-Ga at 3% strain.

boundary distribution and from the vertical magnetic domain feature is magnified in the inset to show the local orientation of magnetic moments. In the regular twin boundary region the magnetic moments within the twinned regions were oriented parallel to the axis of easy magnetization i.e. the magnetic moments arrangement was such that they form 90° domain walls across the twin boundaries (blue (\rightarrow) followed by green (\downarrow) across the twin boundaries). This pattern continued across the entire length of the sample except where the twins interact with a vertical magnetic domain boundary. The red circles highlight regions where twin boundaries and the vertical magnetic domain boundaries interact. Here, the 90° domain walls no longer existed. In this region, irrespective of the twin boundaries, all the magnetic moments aligned horizontally. Within the twins, the magnetic domains tended to orient at a certain angle pointing upwards and approximately parallel to the twin boundaries. Fig. 9 shows the individual magnetic energy distribution for the regular twin boundary region and the vertical domain feature. The anisotropy energy in the regular twin boundary region was significantly lower compared to that in the vertical magnetic domain feature. Right at the intersection of the twin boundary and the vertical domain wall there were high concentrations of anisotropy energy



Magnetic moment orientation

Fig. 6. Equilibrium magnetic domain structure for a single twin boundary in the sample. The orientation of magnetic moments at the twin boundary and the domain boundary are magnified in the regions indicated by rectangles. The line inclined at 45° is the twin boundary. The c-axis (axis of easy magnetization) in this case is defined to be parallel (horizontal) in the left twin domain and perpendicular (vertical) in the right twin domain with respect to the length of the sample. Within these twin domains, the magnetic moments are aligned parallel to the c-axis and form 180° (anti-parallel) domains walls. These 180° from the adjacent twin domains tend to connect at the twin boundary, thereby resulting in a 90° domain wall. Colors red (\leftarrow), blue (\rightarrow), yellow (\uparrow) and green (\downarrow) represent the direction of magnetic moments. The arrows in the magnified sections reveal vortices of the local magnetic moments. (For interpretation of the references to color in this figure legend, the reader is referred to the web version of this article.)

and also the alternating regions within the vertical domain feature had high anisotropy energy.

The total magnetic energy (sum of anisotropy, exchange, and stray field energy) for a single twin boundary system is compared to a dense twin boundary system in Fig. 10. The distribution of magnetic energy was uniform (and low) throughout the sample except at transition regions (twin boundaries and magnetic domain boundaries) for the single twin boundary system. Whereas in a dense twin boundary system with multiple vertical magnetic domains there were localized energy concentrations (\approx 300-400 kJ/m³) at the intersection of the vertical magnetic domain and twin boundaries. In these regions, the magnetic moments stood at a right angle with the direction of easy magnetization (circled regions in Figure 8).

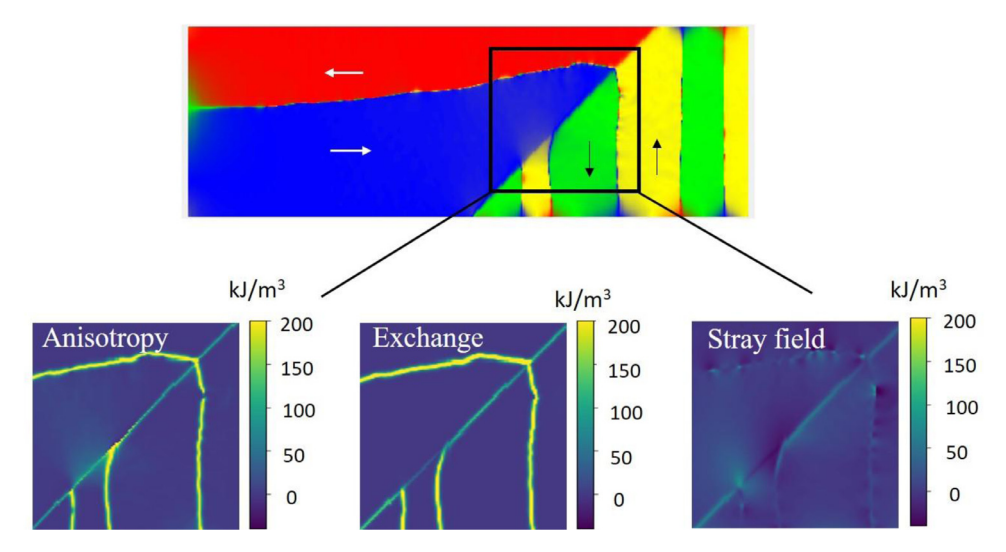


Fig. 7. Magnetic energy distribution for a single twin boundary in the sample. The Anisotropy, Exchange, and Stray field energy are plotted for the selected region from the domain structure.

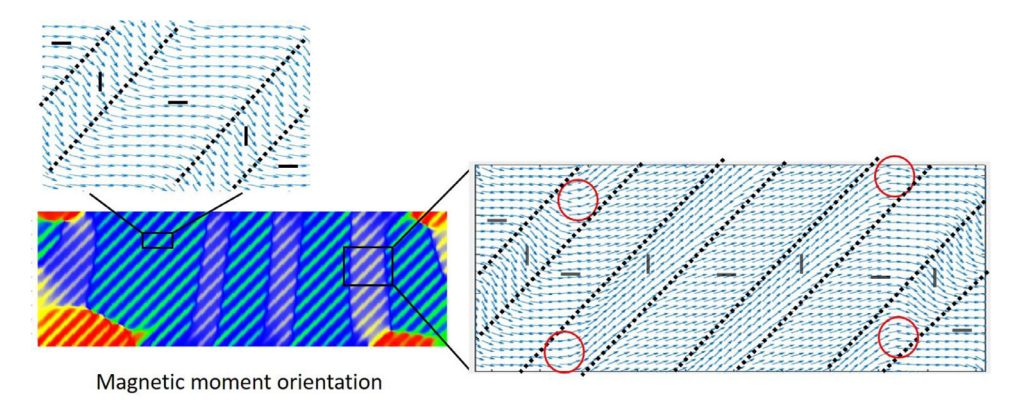


Fig. 8. Equilibrium magnetic domain structure for a dense twin structure in the sample. The orientation of magnetic moments for regular twin boundary region (left inset) and vertical domain regions (right inset) are magnified. The vertical domain regions formed at magnetic domain boundaries that separated the magnetic domains that are oriented down (green) and up (yellow). Colors red (\leftarrow), blue (\rightarrow), yellow (\uparrow) and green (\downarrow) represent the direction of magnetic moments. The black dotted lines are a guide to identify the twin boundaries. The regions of intersection between twin boundary and the vertical magnetic domains are highlighted in red circles, which is where the magnetic moments are aligned perpendicular to the *c*-axis (\uparrow). The alternating horizontal and vertical lines represent the orientation of the *c*-axis (axis of easy magnetization). The arrows in the magnified sections reveal vortices of the local magnetic moments. (For interpretation of the references to color in this figure legend, the reader is referred to the web version of this article.)

5. Discussion

To study the twin boundary mobility in Ni–Mn–Ga with fine twinned structure, we evaluated the mesoscale magnetic defects and the magnetic energies associated with these defects. Here we discuss how these magnetic defects lead to the work hardening in densely twinned Ni–Mn–Ga.

In shape memory alloys, deformation twinning (i.e. the motion of twin boundaries) is the dominant deformation mechanism [30]. The twinning disconnection [31] (or twinning dislocation) is the elemental carrier of localized displacements [32]. As a twinning disconnection moves along the twin boundary, the twin boundary is displaced by the disconnection step height and one twin domain gets displaced with respect to the other twin domain by the Burgers vector.

Three basic mechanisms contribute to the twinning stress in shape memory alloys: (i) the Peierls stress [33], (ii) the nucleation stress for generating twinning disconnections [19], and (iii) the interaction of disconnections with other defects such as other twin boundaries [34] and other twinning disconnections [35]. The threshold stress for the twin boundary mobility depends on twinning disconnections and their interaction with interfaces. When the twinning disconnections come closer to an interface, they have to overcome their mutual repulsive interaction. As they overcome this energy barrier with higher

mechanical stress, the twinning disconnections move further and get stuck at the domain interface in a position of local mechanical equilibrium. In the present study, the energy barriers in a fine twin system are the high concentrations of anisotropy energy (Fig. 9 and also visible in the total magnetic energy plot in Fig. 10b).

High magnetic energy concentrations arise where the twin boundaries interact with the vertical magnetic domains (Fig. 8). These sites form the transition zones (highlighted in circle pattern, Fig. 8) where the magnetic moments are perpendicular to the c-axis (easy axis of magnetization), giving rise to high localized internal magnetostress [26,36]. These regions – we call them magnetoelastic defects – are the same regions that have high concentrations of anisotropy energy (highlighted in oval pattern, Fig. 9). The magnetostress is highest when the magnetic field is perpendicular to c. In such a case, the magnetic field exceeds the saturation field and the maximum shear stress exerted by the magnetic field is $\frac{K}{s}$ (is about 1.37 MPa, where $K = 1.65 \times 10^5$ J/m³ is the anisotropy constant for 5M structure [37] and s = 0.1274 is the twinning shear [20]). The concentration of such magnetoelastic defects increases with increasing twin density. As the twin regions become finer, the contribution of anisotropy energy drastically increases (Fig. 5) thereby increasing the total magnetic energy (Fig. 3). As the twinning disconnections move along the twinning plane, they approach these high energy magnetoelastic defects, which they encounter as obstacles.

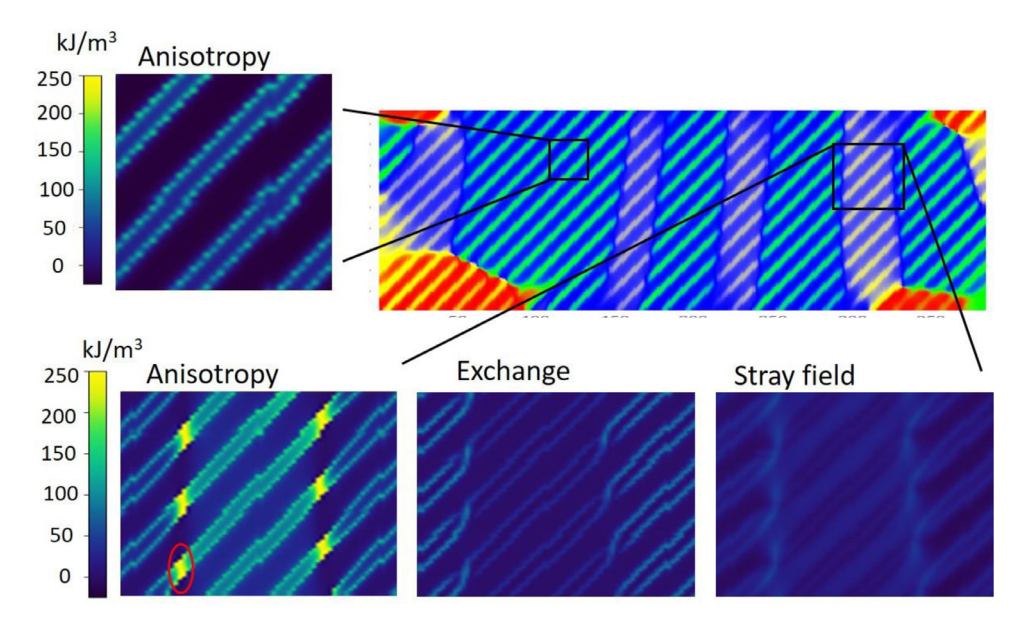


Fig. 9. Individual magnetic energies for a dense twin structure in regular twin boundary region (left square inset) and vertical domain regions (right square inset). The high concentration of anisotropy energy at the intersection of the twin boundary and vertical domain boundary is highlighted in the oval pattern.

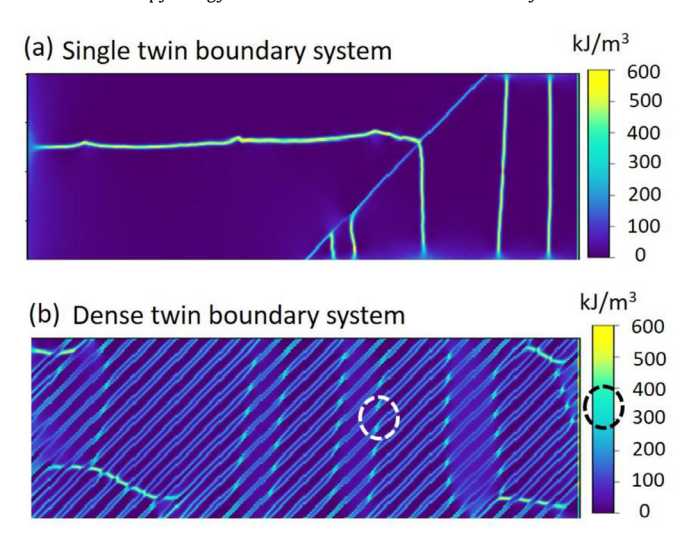


Fig. 10. Total magnetic energy for (a) single twin boundary and (b) dense twin structure in Ni-Mn-Ga. The interaction regions of twin boundary and vertical magnetic domains are highlighted in the energy distribution plot. The magnetic energy at this region is also highlighted on the scale.

The twinning dislocations require higher mechanical stress to move past these magnetoelastic defects.

In regions where the twin boundaries do not interact with the vertical magnetic domain, there are no such energy concentrations (Fig. 10). This is because, across the twin boundaries, the magnetic moments are oriented parallel to their axis of easy magnetization (magnified region in Fig. 8: blue (\leftrightarrow) followed by green (\uparrow)). This results in zero internal magnetostress. Thus, the twinning dislocations move along the twin boundary without encountering any obstacles.

In their statistical model, Glavatska et al. [38] assume a distribution of stress sources in magnetic shape memory alloys. The normal Gauss distribution of the magnetostress effect was used to obtain results for qualitative consideration which lead to this equation:

$$\langle \left(|\sigma_n| - |\sigma_c| \right)^2 \rangle = \sigma_0^2 \tag{3}$$

 $(|\sigma_n| - |\sigma_c|)$ is the critical stress that is needed to overcome the pinning of the twin boundaries. Where, $|\sigma_n|$ is the stress of the n^{th} twin

boundary, $|\sigma_c|$ is the average stress value from the stress distribution curve, and σ_0 is a parameter describing the width of the distribution.

Here, we identify magnetic vortices and the transition regions at the vertical magnetic domain boundaries in densely twinned structures as stress sources. In these regions, the magnetic moments are strongly inclined away from the direction of easy magnetization. Thus, the local magnetic field has a substantial component perpendicular to c and causes a magnetostress [36]. In 2004, Chernenko et al. [26] modified the statistical model that was proposed by Glavatska et al. to theoretically study the magnetoelastic behaviour of Ni–Mn–Ga with single and poly variant microstructures. They use σ_0 = 1.1 MPa i.e. the twinning stress ranges to a maximum of 2.2 MPa. From their stress–strain loops (obtained at magnetic fields higher than saturation), the stress (mechanical stress + magnetostress) at 1.5% for a poly variant Ni–Mn–Ga is 3.25 MPa [26].

With increasing twin density, the density of magnetoelastic defects increase and so does the density of local magnetic stress concentrations. Further, the strength of these magnetoelastic defects is more widely distributed. In addition, with higher twin density, more twinning disconnections contribute to the total deformation. The following deformation path emerges: At the onset of deformation, only those disconnections move, that are far away from a magnetoelastic defect. The motion of these disconnections requires low stress. Eventually, these disconnections encounter a strong magnetoelastic defect and stop moving. Other disconnections start to move at a slightly higher stress. As deformation goes on, more and more disconnections encounter stronger magnetoelastic defects and require higher and higher stress for deformation to proceed. This is the work hardening mechanism in highly twinned Ni-Mn-Ga. As the twin density increases, the obstacle density and the width of their strength distribution increase and, thus, the work hardening coefficient (i.e. the slop of the stress-strain curve) increases. Glavatska et al. and Chernenko et al. found a stress variation of 1-3 MPa [26,38] as discussed above. These stress distributions lead to a corresponding hardening range and agrees well with the mechanical properties reported by Straka et al. (Fig. 1, [21]).

At low twin density, magnetic domain boundaries have high energy and form magnetoelastic defects at twin boundaries (Figs. 6 and 7). However, these defects are very widely spaced such that many twinning disconnections travel between them. These twinning disconnections form dislocation pile-ups. The force on the head dislocation of a pile-up is the regular force exerted by the applied shear stress

multiplied by the number of dislocations in the pile-up ([39], also e.g. [40]). Therefore, the twinning disconnections overcome these defects at very low applied stress. This explains the stress plateau for deformation of samples with only one twin boundary (Fig. 1).

For highly twinned microstructures, only one or a few twinning disconnections travel between two magnetoelastic obstacles. The number of disconnections per obstacle decreases with increasing twin density because the density of defects increases. Thus, the thinner the twins are, the fewer disconnections assist the active dislocation overcoming an obstacle. This further adds to the hardening rate.

6. Conclusions

We evaluated the magnetic domains and twin boundary interactions in Ni-Mn-Ga. We found that as the twinned regions get finer, the magnetic interactions with twin boundaries form magnetoelastic defects with the magentization perpendicular to the axis of easy magnetization. This configuration results in high stress concentrations. The magnetoelastic defects play an important role for twin boundary mobility. The moving twinning disconnections require higher mechanical stress to overcome these local stress concentrations. Thus, magnetoelastic defects act as obstacles for twin boundary motion. In contrast to the dense twin structure, the synergistic action of many twinning disconnections reduces the effectiveness of magnetoelastic defects in microstructures with low twin density. Therefore, in a single twin boundary system or a less dense twin structure, the twin boundaries propagate across the sample with a constant stress. The higher the twin density, the more effectively magnetoelastic defects hinder twin boundary motion. Together with the statistical distribution of defects, these mechanisms result in work hardening. Therefore, the work hardening rate increases with increasing twin density.

Declaration of Competing Interest

None.

Acknowledgments

We would like to acknowledge high-performance computing support of the R2 compute cluster (DOI: 10.18122/B2S41H) provided by Boise State University's Research Computing Department. This research was supported in part by the National Science Foundation under project number DMR-1710640.

Appendix A

Fig. A1.

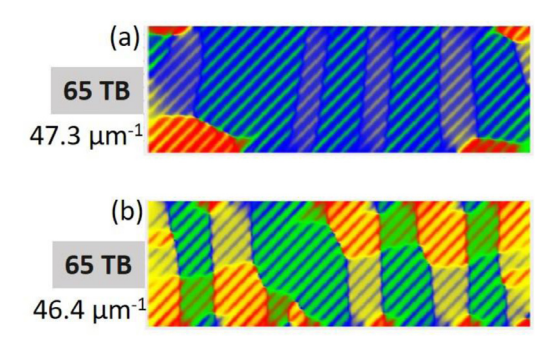


Fig. A1. The equilibrium magnetic domain structures of Ni–Mn–Ga with the formation of vertical magnetic domains at (a) 2% and (b) 4% strain with highest twin density of 47.3 μ m⁻¹ and 46.4 μ m⁻¹ respectively. The colors red (\leftarrow), blue (\rightarrow), yellow (\uparrow), and green (\downarrow) in the figures represent the direction of magnetic moments. (For interpretation of the references to color in this figure legend, the reader is referred to the web version of this article.)

References

- M. Acet, L. Mañosa, A. Planes, Magnetic-field-induced effects in martensitic Heusler-based magnetic shape memory alloys, Handb. Magn. Mater. 19 (2011) 231– 289, doi: 10.1016/B978-0-444-53780-5.00004-1.
- [2] A. Sozinov, N. Lanska, A. Soroka, W. Zou, 12% magnetic field-induced strain in Ni-Mn-Ga-based non-modulated martensite, Appl. Phys. Lett. 102 (2013), doi: 10.1063/1.4775677.
- [3] L. Straka, O. Heczko, H. Hänninen, Activation of magnetic shape memory effect in Ni–Mn–Ga alloys by mechanical and magnetic treatment, Acta Mater. 56 (19) (2008) 5492–5499, doi: 10.1016/j.actamat.2008.07.020.
- [4] P. Müllner, A.H. King, Deformation of hierarchically twinned martensite, Acta Mater. 58 (16) (2010), doi: 10.1016/j.actamat.2010.05.048.
- [5] K. Ullakko, J.K. Huang, C. Kantner, R.C. O'Handley, V.V. Kokorin, Large magnetic-field-induced strains in Ni₂MnGa single crystals, Appl. Phys. Lett. 69 (1996) 1966–1968. doi: 10.1063/1.117637.
- [6] N.J. Kucza, C.L. Patrick, D.C. Dunand, P. Müllner, Magnetic-field-induced bending and straining of Ni–Mn–Ga single crystal beams with high aspect ratios, Acta Mater 95 (2015) 284–290, doi: 10.1016/j.actamat.2015.05.030.
- [7] I. Suorsa, E. Pagounis, Magnetic field-induced stress in the Ni-Mn-Ga magnetic shape memory alloy, 95 (2004) 4958-4961. doi:10.1063/1.1697617.
- [8] A. Sozinov, A.A. Likhachev, N. Lanska, K. Ullakko, Giant magnetic-field-induced strain in NiMnGa seven-layered martensitic phase, Appl. Phys. Lett. 80 (2002) 1746–1748, doi: 10.1063/1.1458075.
- [9] Q. Peng, J. Huang, M. Chen, Effects of demagnetization on Magnetic-Field-Induced Strain and microstructural evolution in Ni–Mn–Ga Ferromagnetic Shape Memory Alloy by phase- field simulations, 107 (2016) 361–370. doi:10.1016/j. matdes.2016.06.050.
- [10] O. Söderberg, Y. Ge, A. Sozinov, S.P. Hannula, V.K. Lindroos, Recent breakthrough development of the magnetic shape memory effect in Ni–Mn–Ga alloys, Smart Mater. Struct 14 (2005), doi: 10.1088/0964-1726/14/5/009.
- [11] O. Heczko, K. Jurek, K. Ullakko, Magnetic properties and domain structure of magnetic shape memory Ni–Mn–Ga alloy, J. Magn. Magn. Mater. 230 (2001) 996–998
- [12] Y. Ge, O. Heczko, O. Söderberg, S.-P. Hannula, V.K. Lindroos, Investigation of magnetic domains in Ni-Mn-Ga alloys with a scanning electron microscope, Smart Mater. Struct. 14 (2005) S211–S215, doi: 10.1088/0964-1726/14/5/007.
- [13] Y.W. Lai, N. Scheerbaum, D. Hinz, O. Gutfleisch, R. Schäfer, L. Schultz, J. McCord, Absence of magnetic domain wall motion during magnetic field induced twin boundary motion in bulk magnetic shape memory alloys, Appl. Phys. Lett. (2007) 90, doi: 10.1063/1.2737934.
- [14] A. Sozinov, Y. Ezer, G. Kimmel, P. Yakovenko, D. Giller, Y. Wolfus, Y. Yeshurun, K. Ullakko, V.K. Lindroos, Large magnetic-field-induced strains in Ni–Mn–Ga alloys in rotating magnetic field, J. Phys. IV France 11 (2001) 311–316.
- [15] Y.M. Jin, Effects of magnetostatic interaction on domain microstructure evolution in magnetic shape memory alloys: phase field simulation, Philos. Mag. (2010) 169–176, doi: 10.1080/14786430902758671.
- [16] O. Heczko, L. Straka, H. Seiner, Different microstructures of mobile twin boundaries in 10 M modulated Ni–Mn–Ga martensite, Acta Mater. 61 (2013) 622–631, doi: 10.1016/j.actamat.2012.10.007.
- [17] L. Straka, A. Soroka, H. Seiner, H. Hänninen, A. Sozinov, Temperature dependence of twinning stress of Type I and Type II twins in 10M modulated Ni–Mn–Ga martensite, 67 (2012) 25–28. doi:10.1016/j.scriptamat.2012.03.012.
- [18] R. Chulist, L. Straka, N. Lanska, A. Soroka, A. Sozinov, W. Skrotzki, Characterization of mobile type I and type II twin boundaries in 10M modulated Ni—Mn—Ga martensite by electron backscatter diffraction, Acta Mater. 61 (2013) 1913–1920, doi: 10.1016/j.actamat.2012.12.012.
- [19] P. Müllner, Twinning stress of type I and type II deformation twins, Acta Mater. 176 (2019) 211–219, doi: 10.1016/j.actamat.2019.07.004.
- [20] A. Sozinov, N. Lanska, A. Soroka, L. Straka, Highly mobile type II twin boundary in Ni–Mn–Ga five-layered martensite, J. Appl. Phys. Lett. 99 (2011) 124103 1–3, doi: 10.1063/1.3640489.
- [21] L. Straka, N. Lanska, K. Ullakko, A. Sozinov, Twin microstructure dependent mechanical response in Ni–Mn–Ga single crystals, J. Appl. Phys. Lett. 96 (2010) 131903 1–3, doi: 10.1063/1.3373608.
- [22] L. Straka, H. Hänninen, A. Soroka, A. Sozinov, Ni-Mn-Ga single crystals with very low twinning stress Ni-Mn-Ga single crystals with very low twinning stress, J. Phys. Conf. Ser. (2011) 303, doi: 10.1088/1742-6596/303/1/012079.
- [23] O. Heczko, P. Vertat, M. Vronka, V. Kopecky, O. Perevertov, Ni–Mn–Ga single crystal exhibiting multiple magnetic shape memory effects, Shape Mem. Superelast. 2 (2016) 272–280, doi: 10.1007/s40830-016-0077-9.
- [24] C.J. Garcia-Cervera, Numerical micromagnetics: a review, Bol. Soc. Esp. Mater. Appl. 0 (2007) 1–33.
- [25] A. Hobza, C.J. García-cervera, P. Müllner, Twin-enhanced magnetic torque, J. Magn. Magn. Mater. 458 (2018) 183–192, doi: 10.1016/j.jmmm.2018.03.014.
- [26] V.A. Chernenko, V.A. L'vov, P. Müllner, G. Kostorz, T. Takagi, Magnetic-field-induced superelasticity of ferromagnetic thermoelastic martensites: experiment and modeling, Phys. Rev. B 69 (2004) 134410 [1–8], doi: 10.1103/Phys-RevB.69.134410.
- [27] D.I. Paul, J. Marquiss, D. Quattrochi, Theory of magnetization: Twin boundary interaction in ferromagnetic shape memory alloys, J. Appl. Phys. 93 (2003) 4561– 4565, doi: 10.1063/1.1561993.
- [28] O. Perevertov, O. Heczko, R. Schäfer, Direct observation of magnetic domains by Kerr microscopy in a Ni–Mn–Ga magnetic shape-memory alloy, Phys. Rev. B (2017) 1–5 95 144431, doi: 10.1103/PhysRevB.95.144431.

- [29] O. Heczko, O. Perevertov, D. Král, M. Veis, I.V. Soldatov, R. Schäfer, Using kerr microscopy for direct observation of magnetic domains in Ni–Mn–Ga magnetic shape memory alloy, IEEE 53 (2017) 1–5.
- [30] K. Otsuka, C.M. Wayman, Shape Memory Materials, Cambridge University Press, U.K. 1998.
- [31] R.C. Pond, B. Muntifering, P. Müllner, Deformation twinning in Ni₂MnGa, Acta Mater. 60 (2012) 3976–3984, doi: 10.1016/j.actamat.2012.03.045.
- [32] J.W. Christian, S. Mahajan, Deformation twinning, Prog. Mater. Sci. 39 (1995) 1–157.
- [33] S. Rajasekhara, P.J. Ferreira, A dislocation model for the magnetic field induced shape memory effect in Ni₂MnGa, Scr. Mater. 53 (2005) 817–822, doi: 10.1016/j. scriptamat.2005.06.003.
- [34] P. Müllner, V.A. Chernenko, G. Kostorz, A microscopic approach to the magnetic-field-induced deformation of martensite (magnetoplasticity), J. Magn. Magn. Mater. 267 (2003) 325–334, doi: 10.1016/S0304-8853(03)00400-1.
- [35] P. Müllner, G. Kostorz, Microstructure of magnetic shape-memory alloys: between magnetoelasticity and magnetoplasticity, Mater. Sci. Forum. 583 (2008)
- [36] P. Müllner, V.A. Chernenko, M. Wolgarten, G. Kostorz, Large cyclic deformation of a Ni-Mn-Ga shape memory alloy induced by magnetic fields, J. Appl. Phys. 92 (2002) 6708-6713, doi: 10.1063/1.1513875.
- [37] L. Straka, O. Heczko, Magnetic anisotropy in Ni–Mn–Ga martensites, J. Appl. Phys. 93 (2003) 8636–8638, doi: 10.1063/1.1555982.
- [38] N.I. Glavatska, A.A. Rudenko, I.N. Glavatskiy, V.A. L'vov, Statistical model of magnetostrain effect in martensite, J. Magn. Magn. Mater. 265 (2003) 142–151, doi: 10.1016/S0304-8853(03)00242-7.
- [39] J.P. Hirth, J. Lothe, Theory of Dislocations, second ed., Krieger Publishing Company, Florida, 1982.
- [40] P. Müllner, C. Solenthaler, A proper model of a deformation twin for twin-intersection problems, Philos. Mag. Lett. 69 (1994) 111–113.